JOURNAL OF PROPULSION AND POWER
Vol. 18, No. 4, July–August 2002

Computational-Fluid-Dynamics Investigation of Aeromechanics

Peter D. Silkowski*
United Technologies Research Center, East Hartford, Connecticut 06108
Chae M. Rhie†
Pratt & Whitney, East Hartford, Connecticut 06108
George S. Copeland‡
United Technologies Research Center, East Hartford, Connecticut 06108
and
James A. Eley§ and James M. Bleeg¶
Pratt & Whitney, Middletown, Connecticut 06457

A computational-fluid-dynamics (CFD) tool was developed and applied to a variety of aeromechanics problems, including both forced response and flutter. This three-dimensional nonlinear, viscous, time-accurate code, in conjunction with a large parallel network, is used to demonstrate the mature capability of CFD-based tools for aeromechanical analyses. Examples of multistage blade-row interaction analyses are presented and compared against detailed experimental data highlighting the fidelity of current CFD tools. Flutter analyses of isolated blade rows are also compared to data and used to demonstrate several classical aeromechanical concepts such as influence coefficients, the destabilizing effect of neighboring blades in cascade flutter, the depiction of an aerodynamic damping map, and the flutter benefit of frequency mistuning. These two capabilities, multistage and flutter, are then combined to examine the effect of multistage interaction on the flutter problem. Finally, the reasons for extending the above modeling to include full-aeroelastic capability are discussed, and an example is presented.

Introduction

AEROMECHANICS is one of the latest fields to benefit from the recent growth of computing methods and power. Before the advent of these capabilities, the aeroelastician's toolbox consisted of empirical, analytical, and semi-analytical methods. Empirical methods of course prevent any bold new designs or concepts because one must stay within the parameter space defined by experience. Analytical and semi-analytical methods, such as Theodorsen's function and Whitehead's LINSUB,[1] are limited in applicability to simple configurations (flat plates with no mean loading).

Advancements in computing capabilities over the past decade have expanded the aeroelastic toolbox to include computational-fluid-dynamics (CFD) methods. Forced response three-dimensional multistage, Euler (Ni and Sharma[2]), and Navier–Stokes (Rai[3,4]) codes have been documented for turbines. Similarly for flutter, two-dimensional linearized potential (Verdon and Casper[5]), Euler (Hall and Crawley[6]), Navier–Stokes (Clark and Hall[7]), and three-dimensional linearized Euler (Hall and Lorence[8]) codes are well chronicled. More recently, three-dimensional nonlinear Euler (Chuang and Verdon[9]) and viscous codes (McBean and Liu[10]) have appeared in the open literature. These CFD aeroelastic tools have two benefits over their predecessors: 1) the removal of some restrictions on geometry and 2) detailed flowfield information throughout the entire domain.

These examples highlight the fact that the ability to create a CFD code for aeroelastic purposes has existed for some time. However, a CFD code by itself is not very useful unless it is fast enough to solve meaningful problems in a timely fashion, that is, during the design cycle. This point is further clarified by comparing the nature of aeromechanical analysis to, for example, steady aerodynamic design, which has already benefited greatly from CFD over the past decade. Normally a steady aerodynamic design is focused at one or perhaps at most two operating points. For example, depending on the mission nature this design point might be either cruise or takeoff. In contrast, aeromechanics requires the examination of several operating conditions, oftentimes well off design. In forced response one might be guided by crossings on the Campbell diagram as to what conditions to examine. Unfortunately, for flutter there is no clear guide, and a wide range of operating conditions, structural mode shapes, and nodal diameter patterns must be examined. Because of this much larger parametric space and the prohibitive amount of time required to calculate these additional conditions, CFD tools have been used mainly for steady design work until recently.

Linearized methods and other modeling techniques such as harmonic balance[11,12] have received much attention in the last few years as potential solutions to this situation. However, this paper will take a different tack and demonstrate that with the corresponding computing facilities a time-accurate viscous code can be applied to a wide range of aeromechanic problems within a meaningful period of time and hence be used as a viable design tool. This direct approach does have drawbacks, mainly circumferential scaling issues such as low nodal diameters for flutter or blade count scaling/matching in multistage analysis. However, this approach is straightforward to implement and removes some of the modeling assumptions made by the preceding methods. Particularly, this allows for the analysis of problems that do not have a well defined steady flowfield or that contain multiple frequencies of interest that are not harmonics of one another and for the development of full aeroelastic models to capture nonlinear fluid structure interactions.

Theory

Rhie's NASTAR code[13] is at the heart of the CAAS (Compressor Analytical Aeromechanics System) tool, which was used for these analyses. NASTAR, a three-dimensional Reynold's-averaged Navier–Stokes, pressure-based code was modified by Silkowski and Rhie for aeromechanical (multistage and flutter) applications.

Received 13 September 2001; revision received 22 January 2002; accepted for publication 30 January 2002.

*Group Leader, Thermal Fluid Sciences, 411 Silver Lane, MS 129-19.
†Fellow, 400 Main Street, MS 163-17.
‡Senior Research Engineer, 411 Silver Lane, MS 129-65.
§Project Engineer, Aircraft Road, MS 401-50.
¶Senior Engineer, Aircraft Road, MS 401-50.

Unsteady multistage capability is provided via direct interpolation between blade rows[2–4] as opposed to previous body force and deterministic stress modeling in the steady multistage code. Flutter calculations are performed on a time-deforming grid, where the blade motion is provided by prescribing a motion based on a structural analysis or by allowing the airfoil to deform freely under the air loads in accordance with a reduced-order structural model (full aeroelastic capability). Both the multistage and flutter capabilities are performed in a time-accurate fashion and model tip clearance by direct gridding.

Results

In this section results are presented in four categories: multistage interaction (forced response), blade-alone flutter, combined multistage flutter, and a fully coupled aeroelastic example. Each of the analyses presented was completed in three days or less, except for the six row example, which took a week. Furthermore, several of these analyses were run simultaneously, demonstrating the timeliness of such analyses within a design effort.

It is expected that the analysis will be in relatively good agreement with known results because significant portions of the relevant physics, specifically, viscosity, time dependence, and tip clearance, have been modeled. Our primary measure of goodness is correctly capturing trends and rankings, with a lesser emphasis on absolute accuracy. To be useful as a design tool, the most important capability is to relatively rank changes. Is configuration "A" better or worse than configuration "B"? Does a given design "tweak" improve or degrade performance relative to the baseline configuration? When large discrepancies are observed with known results, it is most often because of one of three modeling approximations: incorrect geometry such as large scaling of blade counts, poor modeling of system effects/boundary conditions, or an inadequacy in the transition/turbulence models.

Multistage Interaction (Forced Response)

Two examples are given here to demonstrate the use of unsteady CFD to examine multistage interactions. The resultant periodic aeroloads can of course then be combined with structural information to analyze forced response (resonant stress).

The first forced-response/multistage example is the Inlet Guide Vane (IGV) rotor stator of an axial flow compressor. Specifically, comparison is made with the test data of Sanders and Fleeter[14] and Sanders et al.[15] The hardware's blade count ratio of 18:19:18 was modeled in the calculations as 19:19:19. Good agreement was observed between the analysis and the data.

Qualitative agreement is seen in Fig. 1. This figure compares a sequence of "snap shots" of instantaneous Mach contours in the IGV taken on a 90% span radial plane at successive time steps during a period of rotor passing. A distinctive λ feature is clearly visible in both the analysis and the data. This λ pattern is created by the interaction of the incoming rotor leading-edge shock (back portion of λ) and the reflection of a similar shock from the passing of the preceding rotor blade (front portion of λ). Both the data and the analysis reveal that the λ pattern propagates upstream with time. Furthermore, at any instant in time, the CFD and data are quite similar as can be seen by keying off of islands of high and low Mach.

A more quantitative comparison between the CFD and data is seen in Figs. 2–4. Pressure distributions as a function of chord on the suction and pressure sides of the IGV at 90% span are compared in these figures. The maximum, minimum, and time-average envelopes compare favorably in Fig. 2. There is good agreement with data in both the shape and level of the unsteady pressure envelopes. The instantaneous unsteady pressure on the IGV suction and pressure surfaces during one rotor pitch passing are compared in Fig. 3. Overall the agreement is quite good. Specifically, in both the data and CFD one can track the upstream migration of the rotor bow wave. At times in the data, this pulse seems to disappear or weaken; this is caused by the pulse being located between two pressure transducers. Finally, Fig. 4 displays the magnitudes of unsteady pressure at rotor passing and higher harmonics, at a sample axial location on the IGV's pressure surface. Again, the agreement is quite good.

This particular example utilized a model with blade count ratios of 1:1:1 to best match the experimental hardware. However, this is not indicative of any restrictions. In general, multistage analyses utilize

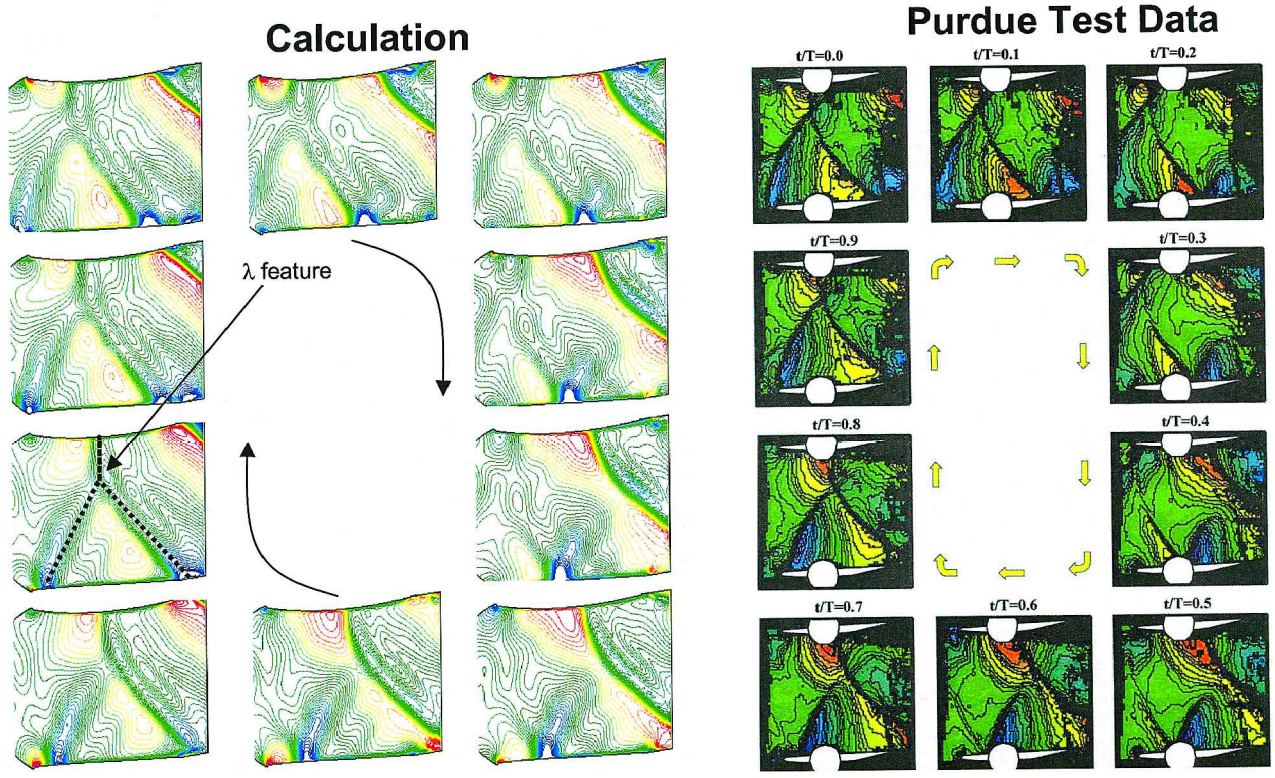

Fig. 1 Instantaneous snap shots in time display good qualitative agreement between the analysis and data, for a top view of Mach at 90% span. Upstream migration of λ structure clearly visible in both sets of figures.

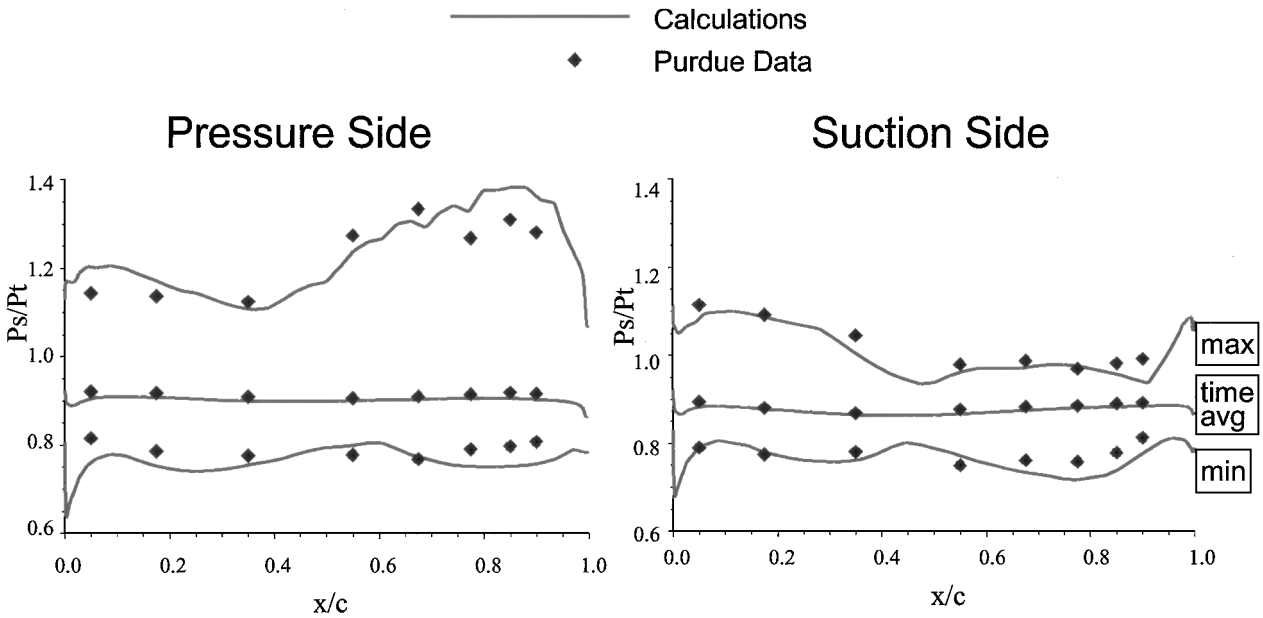

Fig. 2 Comparison at 90% span of unsteady pressure envelope on IGV as a result of rotor passing.

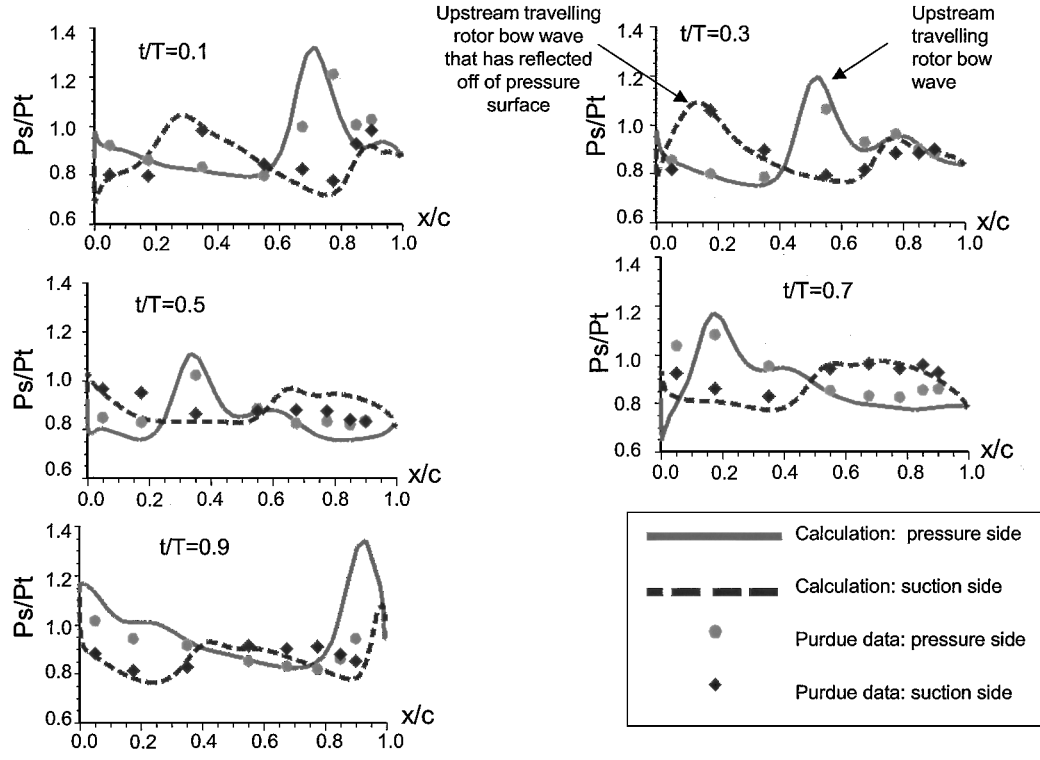

Fig. 3 Analysis matches data in both amplitude and phase for the instantaneous unsteady pressure on the IGV at 90% span. Unsteady pressure is plotted against percent chord. Specifically, tracking with time, both the data and analysis clearly portray the upstream migration of the rotor bow wave.

larger models with blade count ratios on the order of 3:4:5, which are completed in three days. Additionally, even larger models, such as $\frac{1}{8}$th wheel of six blade rows from a compressor with modeled blade count ratios of 4:3:7:5:9:7, are often considered. Figure 5 presents the instantaneous top view of pressure on a radial plane at 23% span for such a case that utilized over 7 million grid points. Blade-related features such as bow waves are clearly visible.

Flutter

In this section several examples of flutter calculations are given. Although many previous authors have demonstrated flutter analyses, few have demonstrated such good agreement with data and the potential of what can be achieved by performing a large number of such calculations. The need for a large number of calculations in flutter analysis is a manifestation of the fact that one does not normally know a priori the most critical flutter conditions, that is, mode shape, nodal diameter pattern, and fan operating conditions (pressure rise and flow). This need to examine a large parametric space has been discussed by several authors. These discussions often include the concept of a flutter or aerodynamic damping map, such as the sketch of Sisto.[16] This diagram indicates that flutter can occur under a wide variety of circumstances, all of which must be investigated.

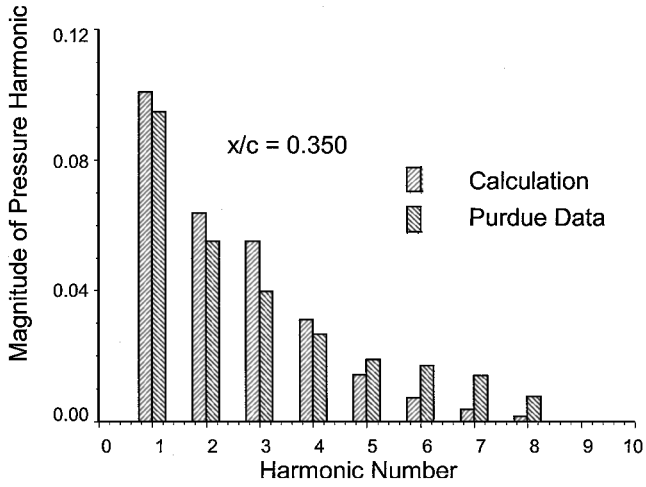

Fig. 4 Quantitative comparison between multistage data and analysis of rotor passing unsteadiness at a sample axial location on the pressure side of the IGV at 90% span. Magnitudes of Fourier transform of unsteady pressure. Because of grid and time-step considerations, only the first few harmonics should really be considered.

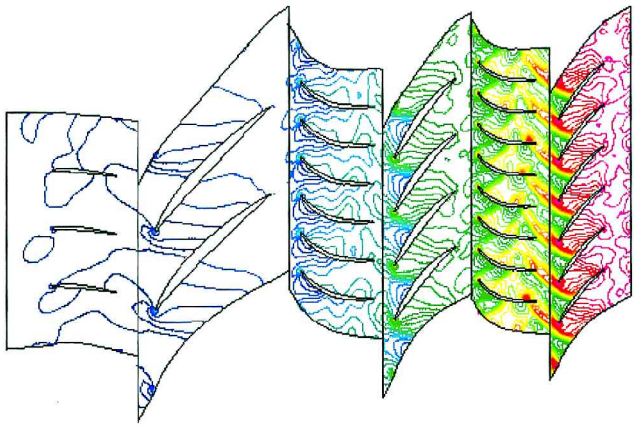

Fig. 5 Top view at 23% span of static-pressure contours through a six-row unsteady multistage calculation. $\frac{1}{8}$th of a wheel calculation with more than 7 million grid points. Bow waves are clearly visible.

Consider now the flutter analysis of a commercial shroudless fan. As an example, calculations were performed on a transonic fan rig operated by Pratt and Whitney and United Technologies Research Center. The configuration modeled a commercial shroudless fan of 16 blades. The fan fluttered in a 0 nodal diameter, first mode (bending) pattern. The frequency of vibration was predicted within 5% of the measured frequency. Figure 6 plots the log decrement of the aerodynamic damping of the mode 1 zero nodal diameter pattern as a function of the mass flow through the fan. Note the good agreement with the experimental data,[17] including the calculation of unstable, negative aerodynamic damping conditions.

Figure 6 also plots the aerodynamic damping for the different nodal diameter patterns at a given flow. Again, there is good agreement with data, including the identification of zero as the limiting nodal diameter. There are many options as to how to model nonzero nodal diameters. One approach combines a single passage domain with time-lagged boundary conditions. However, there is an associated memory and convergence rate penalty associated with this method. A more direct approach, which was taken here, is to have a periodic domain. Therefore, for a two-nodal-diameter pattern one-half of the annulus is modeled. An interesting capability of this approach is that nonphysical nodal diameter patterns can be examined. For example, in this analysis a 5.33-nodal-diameter calculation was performed by using a domain of 3 of the 16 blades. This point does lie on the curve, indicating that one might be able to construct curves of aerodynamic damping vs nodal diameter by calculating a few computationally "friendly" nodal diameters.

An alternate approach for calculating the aerodynamic damping as a function of nodal diameter is to utilize the well-known concept of influence coefficients.[18] This method will create a full nodal-diameter sweep with only *one* calculation. To achieve this, the influence coefficients are not obtained from a Fourier transform of multiple analyses, such as in Fig. 6, but rather from a more deliberate interpretation of the influence coefficients. Specifically, a model is made with several blade passages. However, now instead of all of the blades vibrating with a specific phase relationship, as in the direct method, only one blade in the middle of the domain is vibrated. The resultant unsteady pressure signal on each blade can then be recombined with any specified phasing. Thus with one calculation, the rotor's aerodynamic damping can be determined for all nodal diameters by performing a recombination in the frequency domain of the aerodynamic coefficients that were originally calculated in the time domain. Figure 7 demonstrates the agreement between the influence coefficient and direct methods for a 24-bladed commercial fan. This figure depicts the aerodynamic influence felt by the reference blade (blade 0) as a result

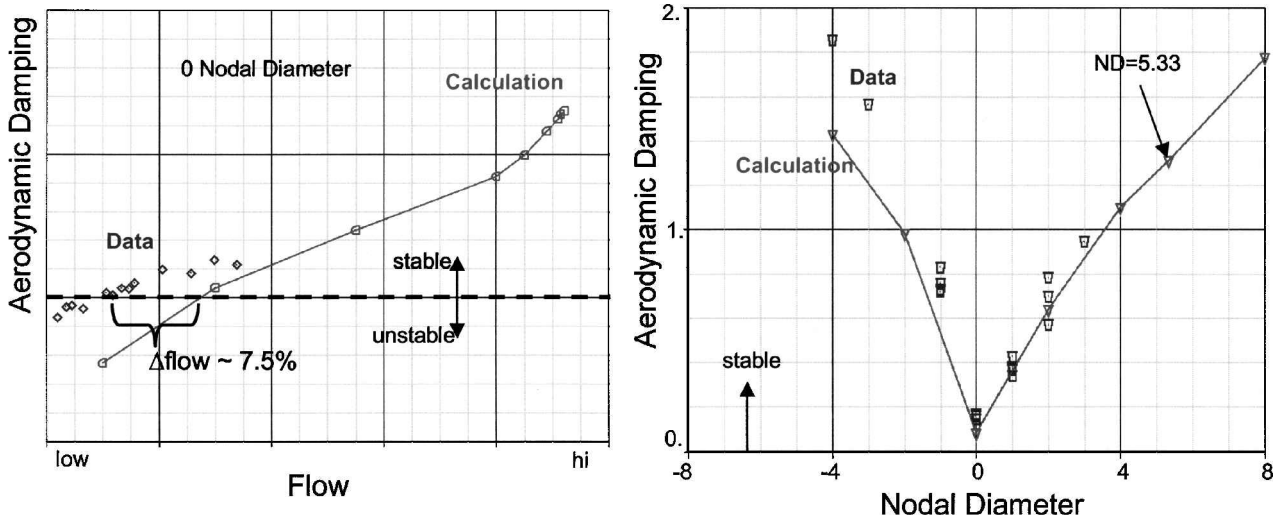

Fig. 6 Comparisons of calculated and measured mode 1 aerodynamic damping for an isolated 16-bladed fan rig that fluttered in 0 nodal diameter. Good trends are observed with both flow and nodal diameter. Note that nonphysical nodal diameter of 5.33 lies along the curve.

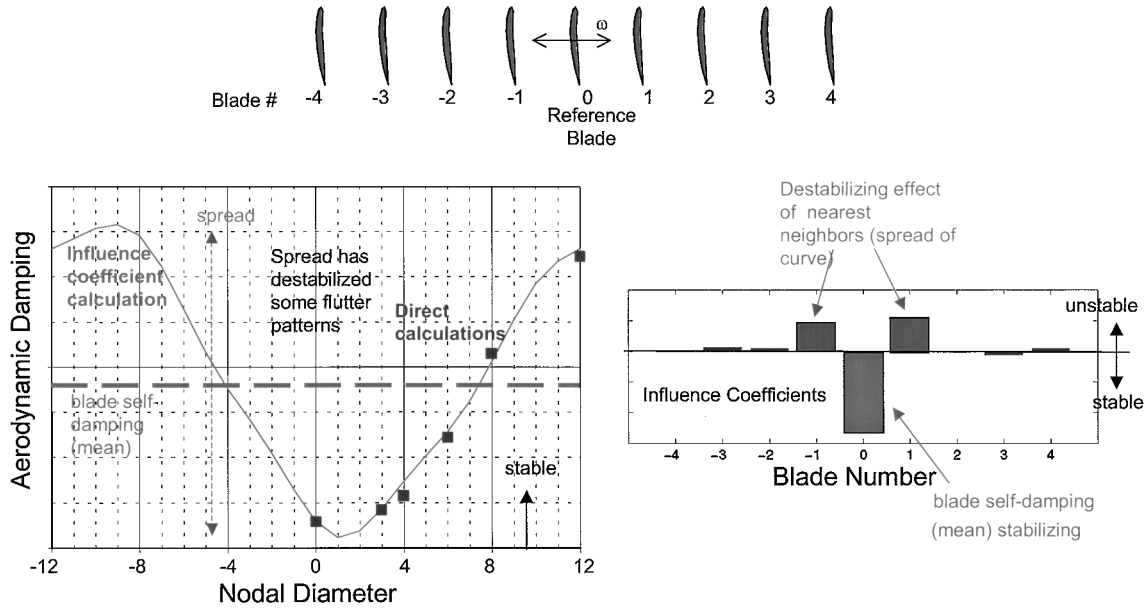

Fig. 7 Aerodynamic damping as a function of nodal diameter calculated for a 24-bladed commercial fan using both the direct and influence coefficient methods. Note the good agreement between the two methods and the traditional dominance of the − 1, 0, 1 influence coefficients, resulting in the familiar sinusoidal plot.

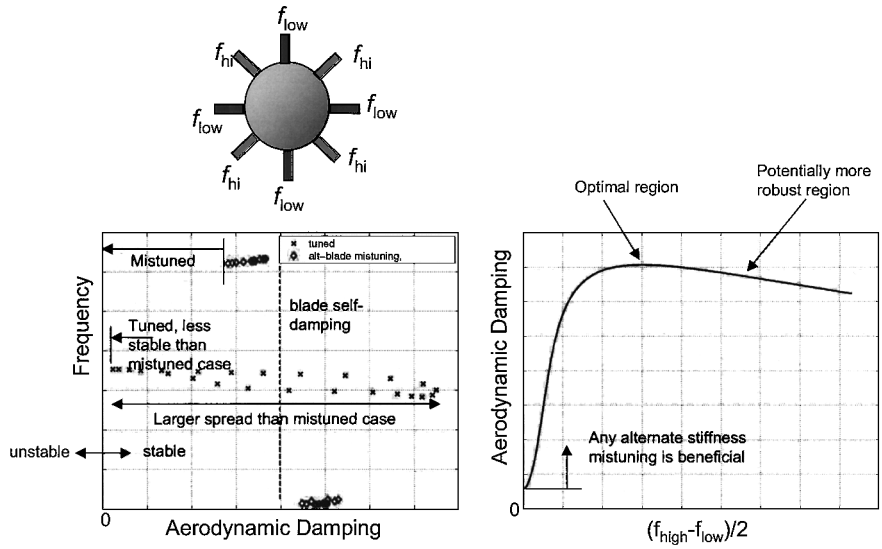

Fig. 8 Sensitivity of aerodynamic damping to intentional mistuning. Alternate-blade mistuning results in two distinct groups of eigenvalues with tighter distributions of damping and more stability than the idealized perfectly tuned example. Each tuned eigenvalue corresponds to a single flutter pattern and is associated with a pure nodal diameter traveling wave. Alternate-blade mistuning eigenvalues are shown for optimal case. The blade self-damping is an upper bound to the max achievable with frequency mistuning. Any alternate mistuning provides a flutter benefit.

of the motion of any of the other blades around the annulus. This influence decays as one moves further away from the reference blade. Finally, the well-known destabilizing effect of cascades is clearly seen in that an individual blade's self-influence is stabilizing while the influence as a result of its nearest neighbors is destabilizing. This calculation also demonstrates the classical result of a sinusoidal damping vs nodal-diameter curve and corresponding $+1$, 0, -1 dominance of the influence coefficients. This influence coefficient approach is appropriate when the dominant blade-to-blade coupling is aerodynamic. If the vibration mode shapes depend strongly on nodal diameter, then the direct approach should be utilized.

Once these influence coefficients are obtained from a tuned flutter analysis, one can quickly examine the effect of stiffness (frequency) mistuning on the flutter characteristics of the blade row. Stiffness mistuning can be implemented through a perturbation of the main diagonal of the structural stiffness matrix; thus, the frequency is allowed to vary blade to blade, but the aerodynamic performance and mode shape are uniform. Alternate stiffness mistuning is a systematic method of mistuning that is effective for improving flutter margin. The idea is to disrupt directly the aerodynamic coupling between adjacent blades and reduce the $+1, -1$ first harmonics and spread of Fig. 7. It is supposed that there are two sets of blades, one with higher frequency than the other, and that they are alternately arranged in the wheel $f_{high} - f_{low} - f_{high} - f_{low}$, such that the mean frequency is still the same. Calculations can be conducted to determine the improvement in flutter stability with this frequency difference ($f_{high} - f_{low}$). Figure 8 illustrates how this feature can be used to look at a range of frequencies to find the optimum. This optimal level of mistuning however might not be the most robust, and it might be beneficial to trade some flutter benefit for robustness and choose to operate at some configuration a bit to the right of the

optimal level of mistuning. For the optimal frequency difference the improvement in stability is seen in the distribution of the tuned and mistuned eigenvalues of Fig. 8. Note the greater spread of the eigenvalues and resulting closer proximity to the stability border (relative loss of stability) for the tuned case. Alternate-blade mistuning is not necessarily an optimal arrangement in the sense that there might be many mistuning arrangements with the same mean frequency and lower standard deviation that yield better flutter stabilization. This pattern however has been widely examined and has the advantage of requiring just one additional part.

Another item of interest is sensitivity to small random mistuning. Provided with a standard deviation for the population of blades as a percentage of the nominal blade frequency, 1000 combinations of randomly chosen blade frequencies were analyzed for flutter damping, and the results are plotted alongside the damping for a tuned rotor as shown in Fig. 9. The results from the multiple random mistuning analyses are represented in the shaded band. For any given vector of blade-alone frequencies, there are 24 flutter patterns, and so there are 24,000 individual points total. For these mistuned rotors the flutter patterns do not occur as pure sinusoidal traveling waves, and nodal diameter in this context is based on the mean interblade phase angle and need not be an integer. In every case the tuned results err on the conservative side, that is, any frequency mistuning causes an increase in the limiting aerodynamic damping.

One great advantage of these computational tools is that they provide more than just the aerodynamic damping. These tools provide detailed information about the flowfield physics. For example, plots of local aerodynamic damping are useful to designers as a guide to help them know where specifically on the blade they should focus their attention, hence allowing for local design tailoring.

To further demonstrate the ability of these tools to capture correctly relevant trends, an analysis was performed on a commercial fan for which test data had shown that the limiting mode and nodal diameter differed at low and high speed. The results of the analysis are shown in Fig. 10. The correct limiting mode is predicted at both low and high speed, and the limiting nodal diameter is within ±1.

Finally, although the aerodynamic damping map schematic of Sisto[16] has been presented in many aeromechanic discussions, few have actually created such a map based on analyses. Panovsky and Kielb[19] created a damping map for turbine airfoils with a quasi-three-dimensional linearized Euler code, and here we present an aerodynamic damping map created from multiple three-dimensional nonlinear viscous analyses of a commercial fan in the transonic regime. The transonic flutter "pinch point" is clearly visible in Fig. 11. The predicted flutter boundary, zero aerodynamic damping boundary, is highlighted by a thickened black contour line.

Multistage Flutter

Traditionally, forced response and flutter have been modeled separately. However, in multistage fans and compressors it is clear that the close proximity of neighboring blade rows or inlets could have a profound effect on the flutter characteristics of a given blade row. This effect has been demonstrated[20] using a two-dimensional linearized inviscid model. Here the geometry of this earlier case (configuration D) is adapted to a 6:8:10 bladed count ratio model with a large radius ratio, and the example is calculated using a three-dimensional time domain, nonlinear, viscous code. Figure 12 displays the results. Although these results are not a perfect match to the preceding analysis, the same key trends are observed. Specifically,

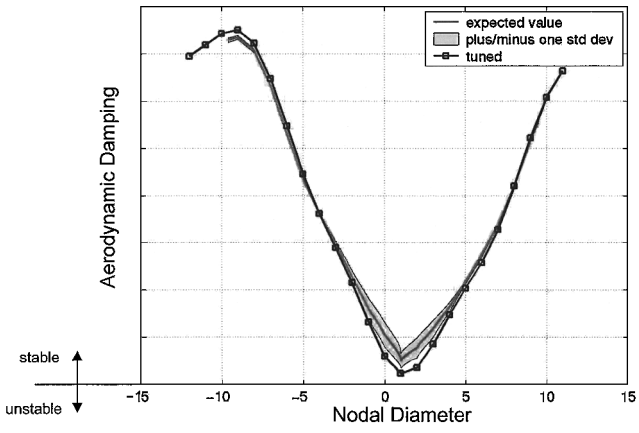

Fig. 9 Sensitivity of aerodynamic damping to random mistuning. The tuned analysis is conservative. Small random frequency mistuning improves aerodynamic damping of the critical nodal diameter. 1000 vectors of random blade frequencies with standard deviation of 0.5% of the nominal blade frequency are considered. Nodal diameter is the average nodal diameter.

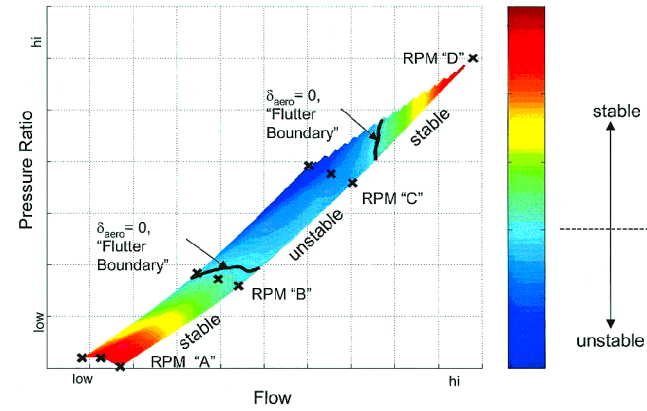

Fig. 11 Conducting calculations at multiple operating lines and rpm (A–D), one can construct an aerodynamic damping map for a commercial fan. Zero aerodynamic damping contours are indicated to highlight the transonic flutter "pinch point."

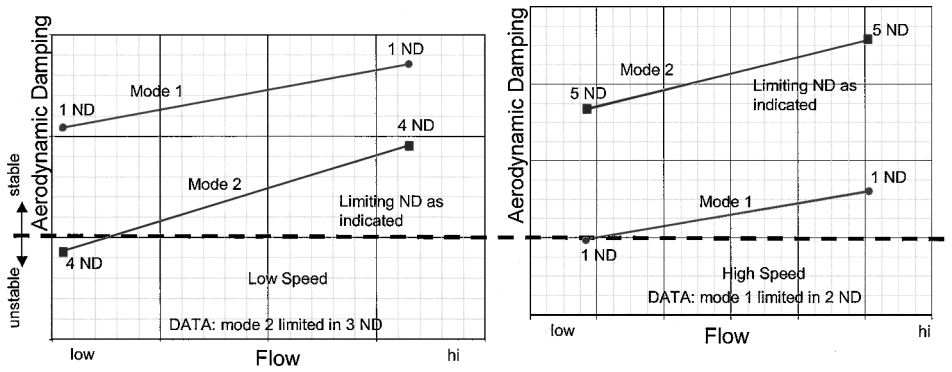

Fig. 10 Comparison of captured trends between calculation and data for a large diameter commercial fan. The calculation correctly captures the change in limiting mode between low and high speed and limiting nodal diameter to within ± 1.

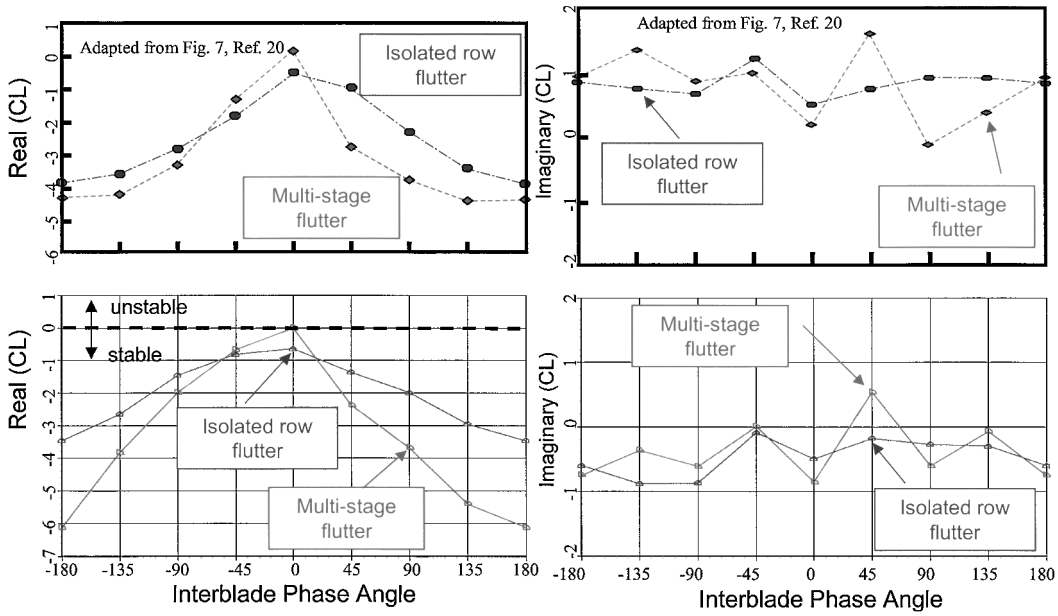

Fig. 12 Calculated real and imaginary components of lift as a function of interblade phase angle for an isolated compressor blade row and the identical blade row in the middle of a three-row multistage model. The difference between the curves represents the importance of including multistage or other "component" effects. —— with open symbols are current work; - - - with filled symbols adapted from Fig. 7 of Ref. 20. Both methods demonstrate similar trends.

considering first the real component of the lift coefficient, the multistage configuration is more stable than the isolated blade row for an absolute value of interblade phase angle greater than 45 deg and vice versa for an absolute value of interblade phase angle less than 45 deg. Furthermore, the zero interblade phase-angle case is the least stable. Additionally, the difference between the multistage and isolated row results is greater for the positive interblade phase angles than it is for the negative interblade phase angles. Now considering the imaginary component of the lift coefficient, the isolated row result contains a peak at an interblade phase angle of −45 deg, flanked by a concave-up segment for smaller interblade phase angles and a concave-down segment for larger interblade phase angles. The multistage result contains local peaks at interblade phase angles of −135, −45, and an absolute peak at 45 deg with dips at 0 and 90 deg. Admittedly the curves are not well defined because of the low amount of resolution in interblade phase angle. Note, to facilitate comparison only results from Ref. 20 at interblade phase angles that are multiples of 45 deg are presented. Furthermore, the data are connected with dashed and solid lines to assist comparison of trends. Two reasons can be suggested for why the methods do not agree exactly. One potential reason for the discrepancy is that the models are not identical. There are geometric differences such as blade count scaling and two- vs three-dimensional effects in addition to the modeling techniques of viscous time domain vs linearized potential. Another possible explanation is that the calculation performed by the previous authors did not include the unsteady multistage interactions as a result of the relative motion of steady flow features. These effects are the unsteadiness described in the forced response section of this paper. An example of such an item is the unsteadiness seen by the stator as a result of the passing of the downstream rotor's steady potential field. This is not a defect in the coupled mode method of Silkowski and Hall,[20] for this effect can easily be included via their external source term. Furthermore, in a linear framework these effects should be orthogonal to the result unless they occur at frequencies that are harmonics of blade vibration.

Fully Coupled Aeroelastic Capability

In the flutter methods so far described in this paper, a predefined blade motion is imposed on the computational model. This predefined motion typically comes from a standard structural analysis. In reality, however, once the structure begins to move in the presence of the fluid unsteady pressure forces begin to act on the structure and thus to affect the motion of the structure. The fluid and the structure form a coupled system. In the earlier examples, however, the coupling or communication was only in one direction, namely the resulting fluid loads created from the prescribed blade motion, or more formally, only addressing the right-hand side of the standard aeroelastic model:

$$m\ddot{x} + c\dot{x} + kx = f_{\text{areo}}(x, \dot{x}, \ddot{x}, \ldots)$$

The next level of modeling, as has already been discussed by several authors,[21,22] is to allow for fully coupled or two-way communication between the fluid and the structure. In a time-domain model this is a straightforward task. At each time step the aerodynamic loads f_{aero} are passed to a structural model, which then solves the entire equation for the new blade position x. This new blade position is passed to the CFD solver, and the process repeats. This process can be simplified by working in modal coordinates and focusing on only the structural modes of interest.

As an example, a typical section model was created that could vibrate in plunge (pure bending). This was a two-dimensional NACA 0012 airfoil at no incidence in a low-Mach-number flow. This example was specifically chosen as a validation/demonstration test bed because the model problem and its solutions are well documented. The airfoil was oscillated at the structural natural frequency for several cycles, and then the forcing was discontinued, and the system allowed to evolve freely. Figure 13 shows a time trace of the airfoil displacement. From the first part of the analysis, the forced harmonic motion, the aerodynamic damping was calculated as C_{aero}, which agreed with the theoretical value. During the free-response portion of the analysis, the log decrement is calculated from successive peaks to correspond to a total damping, which is consistent with the structural damping of the model, specifically, $C_{\text{total}} = C_{\text{aero}} + C_{\text{struc}}$. This capability is useful for three applications. First, in most multistage flutter analyses the phase relationship between the vibration of the airfoils and the relative position of the rotors is not usually known, and in general a sweep of calculations with various phase relationships would have to be conducted to identify the phase that leads to minimal aerodynamic damping. Utilizing this full-aeroelastic capability however facilitates solving this problem with a single calculation in which the blade will choose to

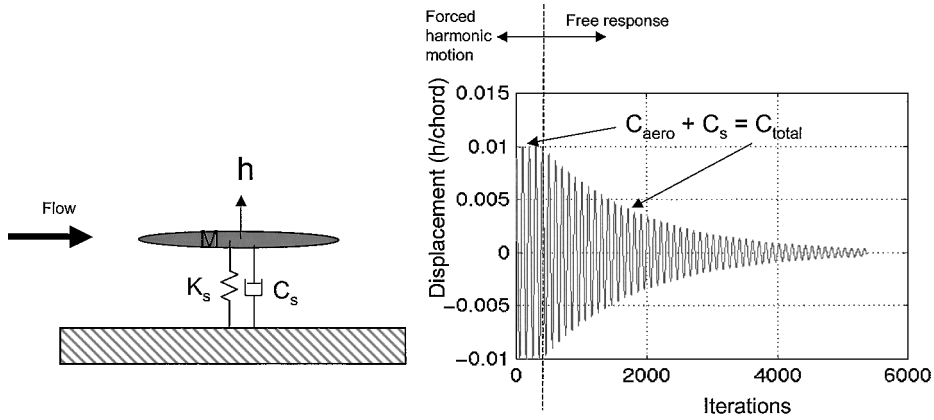

Fig. 13 Fully coupled fluid-structure interaction problem demonstrated on a one-degree-of-freedom plunging symmetric airfoil at low Mach. The structural model was selected to have a damping of C_s and a natural frequency f_0. The airfoil was harmonically forced at this frequency for several cycles, and the theoretical aerodynamic damping C_a was observed. Then the model was allowed to respond freely to the loads at each time step and from the decaying sinusoid; a consistent total damping = $C_s + C_a$ was observed.

vibrate at the phase of least stability. Second, this multistage full aeroelastic analysis can also be viewed as a forced response (resonant stress) problem. However, unlike the resonant stress analysis alluded to in the multistage interaction section, this type of forced response could be considered nonlinear in the sense that the unsteady aerodynamic (multistage loadings and aerodynamic damping) and structural (vibrational frequencies and displacements) analyses are not conducted as separate entities, but instead fall out naturally from a single analysis. Finally, the full aeroelastic capability is needed for some off-design nonintegral vibration problems where interest is in whether or not an unsteady flow feature will lock in with a blade mode, leading to large deflections.

Conclusions

Through a variety of examples in both multistage analysis (forced response) and flutter, this paper has demonstrated that computational software and hardware have both progressed to a level where real aeromechanical problems can be addressed within a computational framework. Several classical concepts such as influence coefficients, an aerodynamic damping map, the flutter benefit of frequency mistuning, and the importance of multistage interactions were demonstrated with fully three-dimensional viscous calculations. Additionally, the extension of these tools into the realm of the fully coupled aeroelastic problem was also demonstrated. It has been shown that given appropriate computational resources a time-accurate approach is a viable tool. Although this approach has several drawbacks, such as circumferential scaling, in the current environment of rapidly increasing computing capability what may have been considered not feasible within a time-accurate method a short while ago is now possible, or might be in the near future. Furthermore, these methods have several potential benefits over alternative modeling approaches. Specifically, these methods are straightforward to implement, relatively robust, and do not contain many of the assumptions and restrictions of other modeling methods. Additionally, these methods easily lend themselves to the full aeroelastic capability, which is a key component for performing multistage flutter analysis, nonlinear resonant stress/forced response, and examining self-induced lock-in phenomena. CFD-based aeromechanical tools have now come of age and can be used to significantly impact real designs.

Acknowledgments

The authors would like to thank the United Technologies/Pratt and Whitney management, particularly those in the Compression Systems Module Center, for their support of this work. Furthermore, the authors wish to acknowledge Mark A. Stephens, Linda Li, Peter C. Bradley, Teresa Sotzing, Ming-Ta Yang, Gary Hilbert, Young-Nam Kim, Robert M. Zacharias, Matthew Montgomery, Timothy A. Wilson, Rachel J. Block, Daniel L. Gysling, Gonzalo Rey, Sanford Fleeter, and Albert Sanders for their contributions.

References

[1]Whitehead, D. S., "Classical Two-Dimensional Methods," *AGARD Manual on Aeroelasticity in Axial Flow Turbomachines, Unsteady Turbomachinery Aerodynamics*, edited by M. F. Platzer and F. O. Carta, Neuilly-Sur-Seine, France, Vol. 1, AG-298, AGARD, 1987, Chap. 3.

[2]Ni, R.-H., and Sharma, O., "Using 3D Euler Flow Simulations to Assess Effects of Periodic Unsteady Flow Through Turbines," AIAA Paper 90-2357, July 1990.

[3]Rai, M. M., "Three-Dimensional Navier–Stokes Simulations of Turbine Rotor- Stator Interaction, Part I—Methodology," *Journal of Propulsion and Power*, Vol. 5, No. 3, 1989, pp. 305–311.

[4]Rai, M. M., "Three-Dimensional Navier–Stokes Simulations of Turbine Rotor-Stator Interaction, Part II—Results," *Journal of Propulsion and Power*, Vol. 5, No. 3, 1989, pp. 312–319.

[5]Verdon, J. M., and Casper, J. R., "Development of a Linear Unsteady Aerodynamic Analysis for Finite-Deflection Subsonic Cascades," *AIAA Journal*, Vol. 20, No. 9, 1981, pp. 1259–1267.

[6]Hall, K. C., and Crawley, E. F., "Calculation of Unsteady Flows in Turbomachinery Using the Linearized Euler Equations," *AIAA Journal*, Vol. 27, No. 6, 1989, pp. 777–787.

[7]Clark, W. S., and Hall, K. C., "A Time Linearized Navier–Stokes Analysis of Stall Flutter," American Society of Mechanical Engineers, Paper 99-GT-383, June 1999.

[8]Hall, K. C., and Lorence, C. B., "Calculation of Three-Dimensional Unsteady Flows in Turbomachinery Using the Linearized Harmonic Euler Equations," *Journal of Turbomachinery*, Vol. 115, No. 4, 1993, pp. 800–809.

[9]Chuang, H. A., and Verdon, J. M., "A Nonlinear Numerical Simulation for Three-Dimensional Flows Through Vibrating Blade Rows," American Society of Mechanical Engineers, Paper 98-GT-18, June 1998.

[10]McBean, I., and Liu, F., "A Three Dimensional Navier–Stokes Code for Aeroelasticity in Turbomachinery," *Proceedings of the 9th International Symposium on Unsteady Aerodynamics, Aeroacoustics and Aeroelasticity of Turbomachines*, edited by P. Ferrand and S. Aubert, ISUAAAT, Lyon, France, Sept. 2000, pp. 709–720.

[11]Chen, T., Vasanthakumar, P., and He, L., "Analysis of Unsteady Blade Row Interaction Using Nonlinear Harmonic Approach," American Society of Mechanical Engineers, Paper 00-GT-431, May 2000.

[12]Hall, K. C., Thomas, J. P., and Clark, W. S., "Computation of Unsteady Nonlinear Flows in Cascades Using a Harmonic Balance Technique," *Proceedings of the 9th International Symposium on Unsteady Aerodynamics, Aeroacoustics and Aeroelasticity of Turbomachines*, edited by P. Ferrand and S. Aubert, ISUAAAT, Lyon, France, Sept. 2000, pp. 409–426.

[13]Rhie, C. M., Gleixner, A. J., Spear, D. A., Fischberg, C. J., and Zacharias, R. M., "Development and Application of a Multistage Navier–Stokes Solver, Part 1: Multistage Modeling Using Bodyforces and Deterministic Stresses," American Society of Mechanical Engineers, Paper 95-GT-342, June 1995.

[14]Sanders, A. J., and Fleeter, S., "Experimental Investigation of Rotor-Inlet Guide Vane Interactions in a Transonic Axial-Flow Compressor," *Journal of Propulsion and Power*, Vol. 16, No. 3, 2000, pp. 421–430.

[15] Sanders, A. J., Papalia, J., and Fleeter, S., "A PIV Investigation of Rotor-IGV Interactions in a Transonic Axial-Flow Compressor," AIAA Paper 99-2674, June 1999.

[16] Sisto, F., "Introduction and Overview," *AGARD Manual on Aeroelasticity in Axial Flow Turbomachines, Unsteady Turbomachinery Aerodynamics*, edited by M. F. Platzer and F. O. Carta, Neuilly-Sur-Seine, France, Vol. 1, AG-298, AGARD, 1987, Chap. 1.

[17] Banaszuk, A., Gysling, D., and Rey, G., "Active Control of Flutter in Turbomachinery Using off Blade Actuators and Sensors," 15th International Federation of Automatic Control World Congress, Barcelona, Spain, July 2002.

[18] Crawley, E. F., "Aeroelastic Formulation for Tuned and Mistuned Rotors," *AGARD Manual on Aeroelasticity in Axial-Flow Turbomachines*, edited by M. F. Platzer and F. O. Carta, Neuilly-Sur-Seine, France, Vol. 2, AG-298, AGARD, 1988, Chap. 19.

[19] Panovsky, J., and Kielb, R. E., ASME Gas Turbine Award, "A Design Method to Prevent Low Pressure Turbine Blade Flutter," American Society of Mechanical Engineers, Paper 98-GT-575, June 1998.

[20] Silkowski, P. D., and Hall, K. C., "A Coupled Mode Analysis of Unsteady Multistage Flows in Turbomachinery," American Society of Mechanical Engineers, Paper 97-GT-186, June 1997.

[21] Carstens, V., and Belz, J., "Numerical Investigation of Nonlinear Fluid- Structure Interaction in Vibrating Compressor Blades," American Society of Mechanical Engineers Paper 00-GT-381, May 2000.

[22] Gnesin, V., Rzadkowski, R., and Kolodyazhnaya, L., "A Coupled Fluid-Structure Analysis for 3D Flutter in Turbomachines," American Society of Mechanical Engineers, Paper 00-GT-380, May 2000.